2024, 21(7): 2433-2439
https://doi.org/10.21123/bsj.2023.8336
P-ISSN: 2078-8665 - E-ISSN: 2411-7986
Baghdad Science Journal

Growth of Different Zinc Oxide Nanostructures under Hydrothermal pH Values

Saja A. H. Abbas [1], ***Ehssan S. Hassan*** [2], ***Oday M. Abdulmunem**** [2]

[1]Ministery of Education, Directorate General for Education, Baghdad, Iraq.
[2]Department of Physics, college of Science, University of Mustansiriyah, Baghdad, Iraq.
*Corresponding Author

Received 06/01/2023, Revised 07/07/2023, Accepted 09/07/2023, Published Online First 25/12/2023, Published 1/7/2024

Abstract

Flower- and rod-like nanostructures of zinc oxide were prepared by the hydrothermal method at 90°C for three hours. Three 0.028 molar solutions, with pH values of 9, 10, and 11, were deposited on glass substrate/ZnO seed layers. All the prepared samples had a polycrystalline diffraction pattern with dominant diffraction from the (002) plane. With increasing pH, the crystallite size increased to a maximum of 37.6 nm. The importance of the research lies in the growth of different nanostructures of zinc oxide by controlling the degree of pH, as the results showed the emergence of flower structures ZnO NFs at pH 11 with a particle size of 100-800 nm, and the development of nanostructures in the form of a bundle of rods at pH 10 with a particle size of 500-800 nm and the development of ZnO NRs in the form of solitary rods perpendicular to the surface at pH 9, with a grain size of 70-80 nm. The optical properties showed a decrease from 78.75% to 79.32% as the pH was increased from 9 to 11, and the value of the energy gap increased from 3.18 eV to 3.31 eV with the increase in the pH value from 9 to 11.

Keywords: Flowerlike, Nanostructure, Rodlike, Seed layer, ZnO hydrothermal.

Introduction

ZnO has a substantial exciton binding energy of 60 meV at ambient temperature and a direct band gap of 3.37 eV, and has potential applications in many areas[1,2], Combining blue–green optoelectronic and UV lasers devices[3], conductive oxides, antistatic coatings, sensors, touch displays, panels and high band gap optoelectronic devices[4,5]. Zinc oxide nanomaterials have been extensively investigated for use as luminescent materials, photocatalysts, surface acoustic wave filters, solar cells, and piezoelectric transducers and actuators[6-8]. ZnO has high chemical and thermal stability. It is also transparent to visible light[7, 9, 10], has high conductivity 2.7 ($S.cm^{-1}$)[11] at 25°C, and exhibits piezoelectric and pyroelectric properties. The properties of ZnO are highly dependent on the specific growth conditions[9, 11]. Therefore, it can form different nanostructures to other metal oxides and is more versatile[5, 12, 13].

One-dimensional ZnO nanostructures, such as nanowires, nanobelts, and nanorods have attracted a lot of interest because of their huge potential in gas sensing applications, including but not limited to their high surface-to-volume ratio.[14-16]. Thermal evaporation, hydrothermal synthesis, sputtering, pulsed laser deposition, and molecular beam epitaxy are a few of the methods used to create ZnO nanostructures that have been reported[17]. Due to its distinct benefits, the hydrothermal approach has received a lot of attention. It is a straightforward, low-temperature 60–100°C, high-yield, and readily controlled process. [18-20]. The synthesis of ZnO nanorods has received much attention in recent years. Cao P. et al.[21], synthesized vertically aligned ZnO nanorods and used them to create C_2H_5OH sensors with good response repeatability. Manabeng M et al.[22], studied an assembly of ZnO flowers and nanorods, fabricated using the hydrothermal method, focusing on morphology-dependent gas sensing properties. Abdulmunem et al.[7], characterized the optical properties of ZnO when doped with Al. Sakata, K. et al. [23] evident that Further increase pf pH leads to a growth of well-defined crystals arranged in flower-like arrangements. Rizwan Wahab, et al.[24] report that sheet/plate like structure when synthesized at the solution pH 6. Thick sheet like structure pH 7. Sheet-like structure to sort of aligned plate and rod like structure is evident at pH 8. Rounded individual sheet to micro flowers pH 9. Bunches of micro flowers were observed with two-dimensional flat surface shape to pH 10. In this work, we aimed to find a correlation between the structure and alignment of ZnO nanorods and the pH of the aqueous solution in which they were formed.

Materials and Methods

In the first stage, a layer of zinc oxide was deposited on glass substrates with dimensions 7.00 × 2.5 cm^2 using the RF magnetron sputtering method. The deposition conditions were base pressure 2.15×10^{-5} torr, substrate temperature 25–27°C, sputtering pressure 1.72×10^{-2} torr and deposition rate 2.42 nm/min. Next, the resulting sample was annealed at 100°C for one hour at atmospheric pressure in grade 304 stainless steel furnace. The structural and surface roughness were examined by field emission scanning electron microscopy (FESEM) and X-ray diffraction (using a JSM-7610F scanning electron microscope and a DJ-3500 X-ray diffractometer). A UV/visible scanning spectrophotometer (Shimadzu UV-1800) was used to record the absorbance spectra in the wavelength range of 300–900 nm. The growth solutions were prepared by adding 1, 1.5 and 1.8 ml of ammonia (Thomas Baker 29% NH_3) to 80 ml of deionized water (BI Supply Deionized Water) to obtain a PH of 9, 10 and 11 respectively, which was measured using an LCD digital pH meter (accuracy 0.01, operating temperature 0–60°C). Zinc nitrate $(ZnO\,(NO_3))_2{\cdot}6H_2O$, PIOCHEM, molar mass 297.47 g/mol) of 99.99% purity was added to the growth solution at a concentration of 0.028 mol/l.

The solution was formed by using a magnetic stirrer at room temperature 25–30°C for 15 minutes, then added to a Teflon cell. The ZnO seed layer was fixed in a Teflon holder horizontally, as shown in Fig. 1, with the zinc oxide seed layer facing downwards, so that all the samples were immersed in the growth solution. Next, the Teflon cell was transferred to a stainless-steel autoclave 200 ml capacity, which was closed tightly and placed in an oven at a temperature of 90°C for three hours. Finally, the samples were removed and left to cool down gradually.

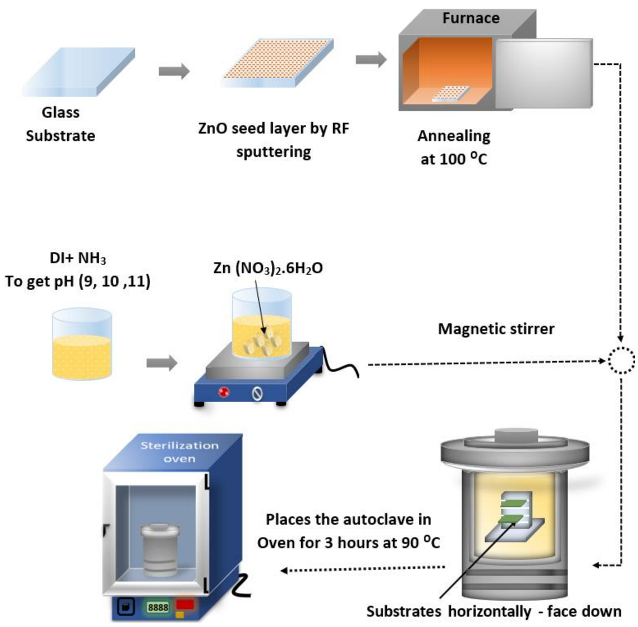

Figure 1. Illustration the steps of preparing ZnO nanorods by hydrothermal system with the stainless-steel autoclave.

Results and Discussion

In the Fig. 2 shows the X-ray diffraction pattern of the zinc oxide nanostructures deposited on glass/ZnO seed layer substrates by the hydrothermal method, for aqueous solutions of pH 9, 10 and 11. It can be seen from Fig. 2 that the diffraction pattern for all models is polycrystalline with a wurtzite ZnO structure pattern and a dominant reflection of the plane (002) at angle 2θ = 34.42°, in addition to several secondary reflections (100), (101), (102), (110), (103) and (200) at angles 31.86°, 36.37°, 47.84°, 56.67°, 62.95° and 66.28°, respectively. This result agrees with the JCPDS 36-1451 card and with Rajasekaran P et al. [23]. It can also be seen that the X-ray diffraction pattern of the ZnO seed layer prepared by the RF magnetron sputtering method has a polycrystalline diffraction pattern with a dominant reflection (002). The crystallite size of the dominant reflection (002) can be calculated from the Scherrer formula 1[24]. The crystallite size increased from 31.86 nm to 37.82 nm as the pH of the aqueous solution changed from 11 to 9 as shown in Table 1. This is due to the change of the nanostructures from flowers to rods and the uniform alignment by increasing the intensity of the prevailing reflection. The process of calculating the observed lattice constants and interplanar distances was carried out using Eq. 2[25] from Table 1.

$$D = \frac{k\lambda}{\beta coscos\,\theta} \qquad 1$$

$$\frac{1}{d^2} = \frac{4}{3}\left(\frac{h^2+hk+k^2}{a^2}\right) + \frac{l^2}{c^2} \qquad 2$$

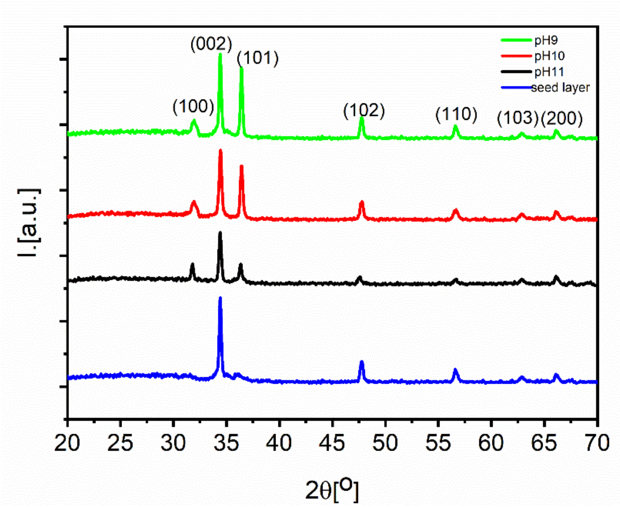

Figure 2. X-ray diffraction of ZnO nanostructure in different aqueous solutions of pH value 9, 10, 11 and ZnO seed layer deposited by RF sputtering.

Table 1. XRD result and structural parameters for ZnO films prepared thermal evaporation in a vacuum.

Sample pH	2θ [º]	(hkl)	Intensity [%]	d value [Å] Observed	d value [Å] JCPDS	lattice constant [Å] Observed a	Observed c	JCPDS a	JCPDS c	crystallite size [nm]
9	34.5	(002)	100	2.284	2.603	3.240	5.208	3.249	5.206	37.82
10	34.5	(002)	100	2.284	2.603	3.240	5.208	3.249	5.206	31.86
11	34.5	(002)	100	2.284	2.603	3.240	5.208	3.249	5.206	32.46
Seed layer	34.5	(002)	100	2.284	2.603	3.240	5.208	3.249	5.206	34.65

In Fig. 3, the FESEM images of ZnO samples that were prepared by hydrothermal method and deposited on a glass/ZnO seed layer substrate submerged in aqueous solutions, at pH (9, 10 and 11). In Fig. 3a–c, the ZnO observed at pH 11, a flower nanostructure formed, and a regular distribution on the surface of the sample. The size of the flower nanostructure ranged from 100 nm to 800 nm. As the pH of the aqueous solution was reduced to 10, as shown in Fig. 3d–f, the nanostructure changed from flowers to semi-rods with a length of 200–900 nm and a diameter ranging between 500–800 nm at the base and 100–200 nm at the top. This is because reducing the pH value reduced the Gibbs free energy, thus nucleation sites become preferred for the occurrence of a regular ZnO growth process[26]. With a decrease in pH to 9, as in Fig. 3h–i, The ZnO semi-rod structures were transformed into compact rods in packs, and it was observed that the diameter of these rods became identical at the base and top, ranging between 70 and 80 nm and the height of the rods reaching 200-300 nm, indicating the regularity of the ZnO nanorods. These results are similar to those of Abass *NK.* [27]. Fig. 3j shows the ZnO seed layer deposited using the RF magnetron sputtering method on glass substrates. At pH 9 ZnONFs first it hydrolyses to produce the OH^- and ammonia. Then, the OH^- forms a complex with Zn^{2+}, followed by thermal decomposition into ZnO. When the pH was increased to 10 (ZnONRs) by adding NH_3, the ammonia into OH^- and NH^{4+} and giving rise to flower-like structure. We believe that by increasing the OH^- ions as compared to Zn^{2+} concentrations immediately start to take place The $[Zn(OH)_4]^{2-}$ acts as the new growth precursor of the nuclei serves on the seed. Therefore, anisotropic growth of ZnO occurs at the active site of ZnO seed[28].

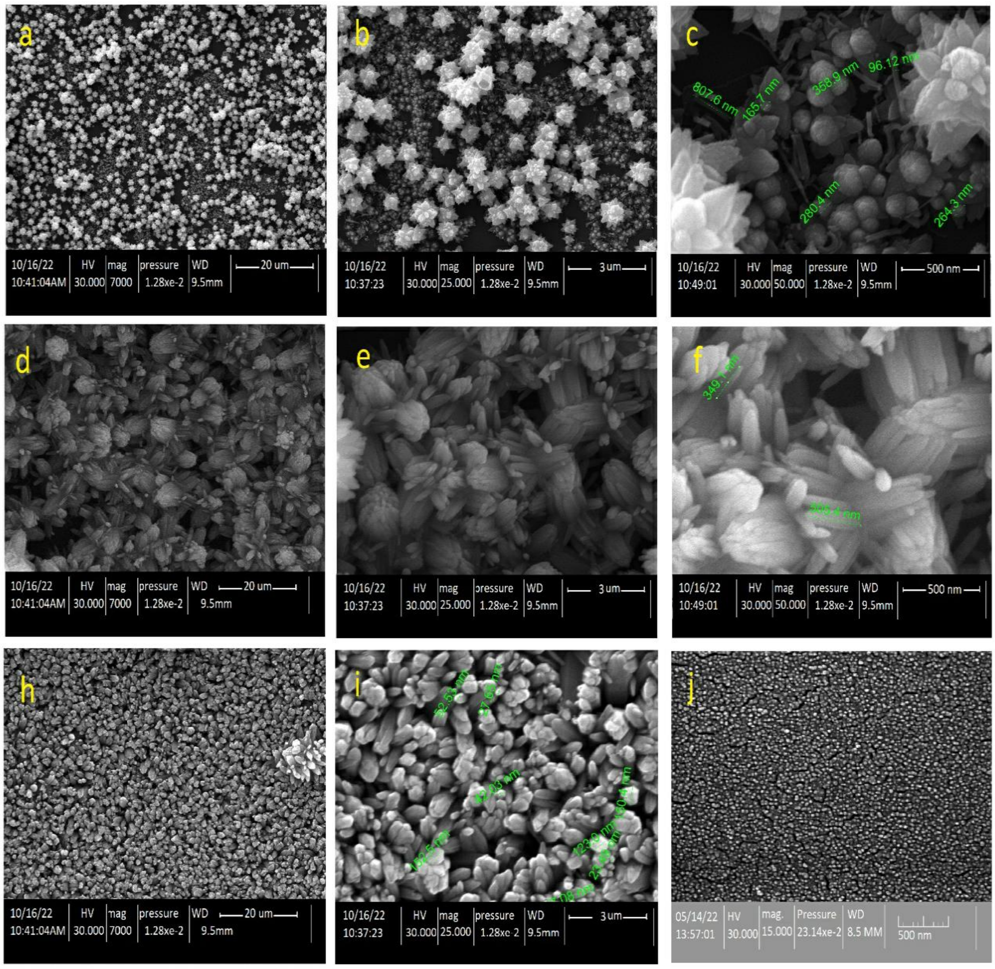

Figure 3. Shows the FESEM image of the ZnO nanoflowers and nanorods prepared by hydrothermal method, (a, b and c) with different aqueous solutions of pH value 11; (d, e and f) at pH value of 10; (h and i) at pH value of 9 and (j) seed layer of ZnO deposited by RF sputtering.

Shown in Fig. 4 is the transmittance spectrum as a function of the wavelength of the ZnO nanostructure samples prepared by the hydrothermal method, with aqueous solutions of pH 9, 10 and 11 and deposited on glass/ZnO seed layer substrates. It can be seen from Fig. 4 that the transmittance spectrum decreased from 89.67% to 79.32% as the pH increased from 9 to 10. This is due to the increase in crystallite size and crystallinity, as well as the change in the shape of the nanostructure from flower to rod. The transmittance spectrum is confined to the visible and near-infrared regions. Fig. 5 illustrates the connection between $(\alpha h\upsilon)^2$ and the photon energy $h\upsilon$, where the value of the energy gap can be calculated by extrapolating the linear portion of the curve and setting the value of the magnitude of the energy gap value being derived by extrapolating the linear component of the curve and setting the magnitude $(\alpha h\upsilon)^2 = 0$ as in Eq. 3[29,30].

$$(\alpha h\vartheta)^2 = B(h\vartheta - E_g^{opt.})^r \qquad 3$$

Moreover, the value of the energy gap increased from 3.18 eV to 3.31 eV with the increase in the pH value from 9 to 11, which also agrees with Zainelabdin A. [31,32]. This effect is due to the change in nanostructure forms from the flower- to rodshaped, which reduces the transmittance while increasing the absorbance [33].

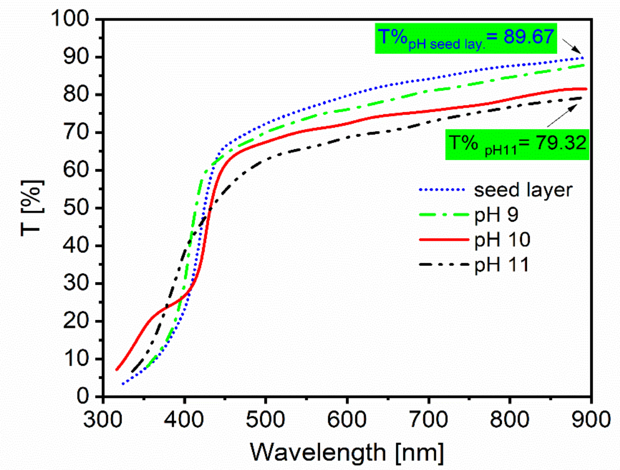

Figure 4. Shows the transmittance percentage of the ZnO nanoflowers and nanorods prepared by hydrothermal method with different aqueous solutions of pH value 9, 10 and 11.

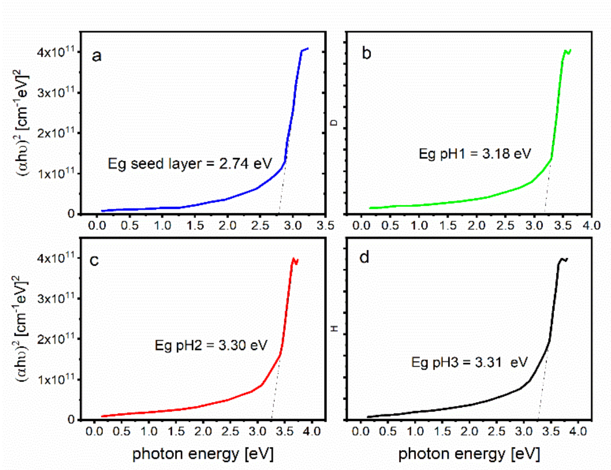

Figure 5. shows the $(\alpha h\upsilon)^2$ as function to photon energy [eV]of the ZnO nanoflowers and nanorods prepared by hydrothermal method with a variety of aqueous solutions of pH value (a) ZnO seed layer, (b) at pH value of 9, (c) at pH value of 10, (d) at pH value 11.

Conclusion

It was found that the pH of the aqueous solution has a significant effect on the shape of ZnO nanostructures deposited on a glass/ZnO seed layer by the hydrothermal method. The nanostructures changed from flower-shaped structures with a diameter of 100–800 nm to rod structures non-perpendicular to the surface of the substrate with a diameter of 500–800 nm and a height of 200–900 nm. At pH 9, the rod nanostructures turned perpendicular to the substrate, in an organized and homogeneous distribution, with a diameter of 200–300 nm and a height of 70–80 nm.

Acknowledgment

The Laboratory of Advanced Materials personnel at the Mustansiriyah University, College of Science is to be thanked and acknowledged by the authors for performing the necessary measurements.

Authors' Declaration

- Conflicts of Interest: None.
- We hereby confirm that all the Figures and Tables in the manuscript are ours. Furthermore, any Figures and images, that are not ours, have been included with the necessary permission for re-publication, which is attached to the manuscript.
- Ethical Clearance: The project was approved by the local ethical committee at the University of Mustansiriyah.

Authors' Contribution Statement

E.S., S.A., and O.M. contributed to the design and implementation of the research, to the analysis of the results and to the writing of the manuscript.

References

1. Kumbhar D, Kumbhar S, Salunke G, Nalawade R. Effect of Cu doping on structural and optical properties of ZnO nanoparticles using sol–gel method. Macromol Symp. 2019; 387(1): 1800192. https://doi.org/10.1002/masy.201800192
2. Verma KC, Goyal N, Kotnala RK. Lattice defect formulated ferromagnetism and UV photo-response in pure and Nd, Sm substituted ZnO thin films. Phys Chem Chem Phys. 2019; 21(23): 12540-54. https://doi.org/10.1039/C9CP02285F
3. Linghu J, Song T, Yang T, Zhou J, Lim K. Computational prediction of stable semiconducting Zn-C binary compounds. Mater Sci Semicond Process. 2023; 155(1): 107237. https://doi.org/10.1016/j.mssp.2022.107237
4. Hassan ES, Abdulmunem OM. Measuring the Response of Annealed Zinc Oxide Thin Films to Ethanol Gas. Braz J Phys. 2022; 52(5): 160. https://doi.org/10.1007/s13538-022-01158-9
5. Elmas S, Pat S, Mohammadi R, Musaoğlu C. Determination of physical properties of graphene doped ZnO (ZnO: Gr) nanocomposite thin films deposited by a thermionic vacuum arc technique. Physica B. 2019; 557(27): 33. https://doi.org/10.1016/j.physb.2018.12.039
6. Habis C, Zaraket J, Aillerie M. Transparent Conductive Oxides. Part II. Specific Focus on ITO, ZnO-AZO, SnO2-FTO Families for Photovoltaics Applications. Defect Diffus Forum.2022; 417(4): 257-272. https://doi.org/10.4028/p-6fqmfi
7. Mikhlif HM, Dawood MO, Abdulmunem OM, Mejbel MK. Preparation of High-Performance Room Temperature ZnO Nanostructures Gas Sensor. Acta Phys Pol A. 2021; 140(4). https://doi.org/10.12693/APhysPolA.140.320
8. Hasanpoor M, Aliofkhazraei M, Delavari H. In-situ study of mass and current density for electrophoretic deposition of zinc oxide nanoparticles. Ceram Int. 2016; 42(6): 6906-6913. https://doi.org/10.1016/j.ceramint.2016.01.076
9. Abdulmuem OM, Ali MJ, Hassan ES. Optical and structural characterization of aluminum doped zinc oxide thin films prepared by thermal evaporation system. Opt Mater. 2020; 109: 110374. https://doi.org/10.1016/j.optmat.2020.110374
10. Alwash A. The green synthesize of zinc oxide catalyst using pomegranate peels extract for the photocatalytic degradation of methylene blue dye. Baghdad Sci J. 2020; 17(3): 0787. https://doi.org/10.21123/bsj.2020.17.3.0787
11. Juraina MD, Ismayadi I, Muhammad RY, Suraya AR. Morphological effect on conductivity performance of ZnO/carbon nanotubes cotton hybrid, Appl Surf Sci. 2022; 7: 100211. https://doi.org/10.1016/j.apsadv.2022.100211
12. Raizada P, Sudhaik A, Singh P. Photocatalytic water decontamination using graphene and ZnO coupled photocatalysts. Mater Sci Technol. 2019; 2(3): 509-529. https://doi.org/10.1016/j.mset.2019.04.007
13. Amakali T, Daniel LS, Uahengo V, Dzade NY, de Leeuw NH. Structural and Optical Properties of ZnO Thin Films Prepared by Molecular Precursor and Sol–Gel Methods. Crystals.2020; 10(2): 132. https://doi.org/10.3390/cryst10020132
14. Wu Wei-Che, Juang Yung-Der. The optical properties of Mg-doped ZnO quantum dots. Solid State Commun. 2022; 350: 114791. https://doi.org/10.1016/j.ssc.2022.114791
15. Wang ZL. Novel nanostructures of ZnO for nanoscale photonics, optoelectronics, piezoelectricity, and sensing. Appl Phys A. 2007; 88(1): 7-15. https://doi.org/10.1007/s00339-007-3942-8
16. Abdussalam-Mohammed W. Comparison of chemical and biological properties of metal nanoparticles (Au, Ag), with metal oxide nanoparticles (ZnO-NPs) and their applications. Adv J Chem A. 2020; 3(2): 192-210. https://doi.org/10.33945/SAMI/AJCA.2020.2.8
17. Nunes D, Pimentel A, Gonçalves A, Pereira S, Branquinho R. Metal oxide nanostructures for sensor applications. Semicond Sci Technol. 2019; 34(4): 043001. https://doi.org/10.1088/1361-6641/ab011e
18. Kaur N, Singh M, Comini E. One-dimensional nanostructured oxide chemoresistive sensors. Langmuir. 2020; 36(23): 6326-6344. https://doi.org/10.1021/acs.langmuir.0c00701
19. Fang X, Bando Y, Gautam UK, Zhai T, Zeng H. ZnO and ZnS nanostructures: ultraviolet-light emitters, lasers, and sensors. Crit Rev Solid State Mater Sci. 2009; 34(3): 190-223. https://doi.org/10.1080/10408430903245393
20. Zhang J, Liu X, Neri G, Pinna N. Nanostructured materials for room-temperature gas sensors. Adv Mater. 2016; 28(5): 795-831. https://doi.org/10.1002/adma.201503825
21. Cao P, Yang Z, Navale ST, Han S, Liu X, Liu W. Ethanol sensing behavior of Pd-nanoparticles decorated ZnO-nanorod based chemiresistive gas sensors. Sens Actuators B Chem. 2019; 298: 126850. https://doi.org/10.1016/j.snb.2019.126850
22. Abbas KN, Bidin N, Sabry RS. Controllable ZnO nanostructures evolution via synergistic pulsed laser ablation and hydrothermal methods. Ceram Int. 2016; 42(12): 13535-13546. https://doi.org/10.1016/j.ceramint.2016.05.146
23. Sakata K, Minhová Macounová K, Nebel R. pH dependent ZnO nanostructures synthesized by hydrothermal approach and surface sensitivity of their photo electrochemical behavior SN. Appl Sci. 2020; 2(2): 203. https://doi.org/10.1007/s42452-020-1975-1

24. Rizwan Wahab, Young-Soon Kim, Hyung-Shik Shin. Synthesis Characterization and Effect of pH Variation on Zinc Oxide Nanostructures. Mater Trans. 2009; 50(8): 2092-2097. https://doi.org/10.2320/matertrans.M2009099
25. Rajasekaran P, Kannan H, Das S, Young M, Santra S. Comparative analysis of copper and zinc based agrichemical biocide products: materials characteristics, phytotoxicity and in vitro antimicrobial efficacy. AIMS Environ. Sci. 2016; 3(3): 439-455. https://doi.org/10.3934/environsci.2016.3.439
26. Manabeng M, Mwankemwa BS, Ocaya RO, Motaung TE, Malevu TD. A Review of the Impact of Zinc Oxide Nanostructure Morphology on Perovskite Solar Cell Performance. Processes. 2022; 10(9): 1803. https://doi.org/10.3390/pr10091803
27. Al-Enizi AM, Shaikh SF, Tamboli AM, Marium A, Ijaz MF, Ubaidullah M, Moydeen Abdulhameed M, Ekar SU. Hybrid ZnO Flowers-Rods Nanostructure for Improved Photodetection Compared to Standalone Flowers and Rods. Coatings. 2021; 11(12): 1464. https://doi.org/10.3390/coatings11121464
28. Amin G, Asif MH, Zainelabdin A, Zaman S, Nur O, and Willander M. Influence of pH, Precursor Concentration Growth Time and Temperature on the Morphology of ZnO Nanostructures Grown by the Hydrothermal Method. J Nanomater. 2011; 10(1155): 269692. https://doi.org/10.1155/2011/269692
29. Agarwal S, Rai P, Gatell EN, Llobet E, Güell F. Gas sensing properties of ZnO nanostructures (flowers/rods) synthesized by hydrothermal method. Sens Actuators B Chem. 2019; 292: 24-31. https://doi.org/10.1016/j.snb.2019.04.083
30. Abass NK, Shanan ZJ, Mohammed TH, Abbas LK. Fabricated of Cu doped ZnO nanoparticles for solar cell application. Baghdad Sci. J. 2018; 15(2): 0198. https://doi.org/10.21123/bsj.2018.15.2.0198
31. Deepak Negi, Radhe Shyam, Srinivasa Rao Nelamarri. Role of annealing temperature on structural and optical properties of MgTiO3 thin films. Mater Lett X. 2021; 11:100088. https://doi.org/10.1016/j.mlblux.2021.100088
32. Zainelabdin A, Zaman S, Amin G, Nur O., Deposition of well-aligned ZnO nanorods at 50◦C on metal semiconducting polymer, and copper oxides substrates and their structural and optical properties. Cryst Growth Des. 2010; 10(7): 3250–3256. https://doi.org/10.1021/cg100390x
33. Amorin LH, Martins LD, Urbano A. Commitment between roughness and crystallite size in the vanadium oxide thin film opto-electrochemical properties.J Mater Res. 2019; 22(1): e20180245. http://dx.doi.org/10.1590/1980-5373-MR-2018-0245

انماء تراكيب نانوية من أكسيد الزنك بطريقة التحلل المائي الحراري لقيم مختلفة من درجة الحامضية

سجى علي حسين عباس [1]، إحسان صلاح حسن [2]، عدي مازن عبد المنعم [2]

[1]المديرية العامة للتربية، وزارة التربية، بغداد، العراق.
[2]قسم الفيزياء، كلية العلوم، الجامعة المستنصرية، بغداد، العراق.

الخلاصة

تم تحضير تراكيب نانوية (زهرية وعصي) الشكل من اكسيد الزنك بالطريقة الحرارية المائية عند 90 درجة مئوية لمدة ثلاث ساعات. تم تحضير ثلاثة محاليل بقيم درجة الحامضية 9 و10 و11 وبمولارية 0.028 مولاري، على قواعد زجاجية / بذور ZnO. كان لجميع العينات المحضرة نمط حيود متعدد التبلور مع حيود سائد من المستوى (002). مع زيادة درجة الحامضية، زاد حجم البلوري إلى حد أقصى قدره 37.6 نانومتر. أظهرت صور الانبعاث الحقلي لمجهر الماسح الإلكتروني تكمن اهمية البحث في انماء تراكيب مختلفة من اكسيد الزنك من خلال التحكم بدرجة الحامضية حيث أظهرت النتائج ظهور تراكيب زهرية عند الحامضية 11 وبحجم جسيمي 100-800 نانومتر، وانماء تراكيب نانوية بشكل حزمة من العصي عند الحامضية 10 وبحجم جسيمي 500-800 نانومتر وانماء اكسيد الزنك بشكل عصي منفردة عمودية على السطح عند الدرجة الحامضية 9 وبحجم حبيبي 70-80 نانومتر. أظهرت الخصائص البصرية انخفاضًا في النفاذية من 78.75 الى 79.32 وزيادة في قيم فجوة الطاقة من 3.18 الكترون فولط الى 3.31 الكترون فولط مع زيادة درجة الحامضية.

الكلمات المفتاحية: الاشكال الزهرية، البنية النانوية، اشكال العصي، طبقة حبيبية، ZnO الحرارية المائية.